

# Radiation Shielding Properties of Nickel, Copper and Iron Based Alloys

Santosh Kumar Das<sup>1</sup>, Saddam Husain Dhobi<sup>2</sup>

<sup>1</sup>Department of Physics, Patan Multiple Campus, Tribhuvan University, Patandhoka, Lalitpur, Nepal

<sup>2</sup>Central Department of Physics, Tribhuvan University, Kirtipur, Kathmandu, Nepal

Corresponding authors: saddam@ran.edu.np/dassantosh29@gmail.com

doi: <https://doi.org/10.3126/ppj.v4i01.70210>

## Abstract

*This study explores the radiation shielding properties of Iron-based and Nickel-based alloys with Cobalt composition to evaluate their performance in photon attenuation and shielding applications. The objectives of this work are to determine linear and mass attenuation coefficients (LAC, MAC), half and tenth value layers (HVL, TVL), mean free path (MFP), effective atomic number and electron density ( $Z_{eff}$ ,  $N_{eff}$ ), effective conductivity ( $C_{eff}$ ), atomic cross section (ACS) and electronic cross section (ECS) of nickel and iron base alloy with Cobalt using Phy-X/PSD within 0.001 MeV to 10 MeV. The result shows Iron and Nickel-based alloys have electron densities around  $10^{23}$  electrons per gram, with increased Iron concentration improving low-energy photon attenuation. Nickel-based alloys have a higher MAC and LAC compared to Iron-based oxides, indicating better photon absorption per unit mass and thickness, respectively. Nickel-based alloys exhibit a lower HVL and TVL, indicating greater attenuation and absorption efficiency for photons, especially at lower energies. Conversely, Iron-based alloys, while showing higher HVL and TVL. Nickel-based alloys exhibited higher electron densities the Iron-based alloys and  $Z_{eff}$  values for Nickel based alloys, ranging from 27.1 to 27.8 while Iron-based alloys with  $Z_{eff}$  between 26.2 and 26.8.  $C_{eff}$  in Iron-based alloys was stable at  $(1.50 \text{ to } 1.74) \times 10^9 \text{ S/m}$ , while Nickel-based alloys showed significant fluctuations below 0.01 MeV. Nickel-based alloys also had higher ACS and ECS, indicating superior photon interaction, especially at lower energies. These results highlight Nickel-based alloys' greater efficacy in low-energy photon attenuation and the stable performance of Iron-based alloys at higher energies.*

**Keywords:** Radiation shielding, iron-based and nickel-based alloys, linear and mass attenuation coefficients, Phy-X/PSD, atomic cross section and electronic cross section

## Introduction

Nuclear energy offers significant advantages in addressing the rising energy demands of a growing global population compared to conventional fossil fuels and renewable sources such as solar and wind, which have issues related to air pollution, global warming, cost, and efficiency (Zhang et al., 2020). Advances in nuclear technology have led to the development of materials capable of withstanding high temperatures and enhancing protection against radiation (Aygün, 2023). Despite these advancements, radiation exposure remains a significant concern, necessitating the development of new, more effective

protective materials. Lead (Pb) has traditionally been used for its high atomic number and density, providing effective radiation shielding, but its drawbacks include poor hardness, low resistance to high temperatures, and toxicity (Hamad, 2023). Alternatives like tantalum (Ta) and tungsten (W) offer better safety and shielding capabilities. Additionally, alloy materials, such as ferroalloys and their high-density variants, present promising options for improved radiation protection due to their enhanced properties (Büyükyıldız et al., 2024). Innovations in nanomaterials, including nickel/cobalt alloys and ferrites, also show potential for superior electromagnetic interference (EMI) shielding and radiation attenuation (Moradi et al., 2024; Alghamdi et al., 2024; Ramakrishna et al., 2024). Furthermore, recent research on glass systems and Ni-based alloys highlights advancements in radiation shielding, demonstrating improved performance through the incorporation of elements like bismuth (Gaber et al., 2024) and the combination of neutron and gamma ray shielding functionalities (Heidarian et al., 2024).

While extensive research has been conducted on the radiation shielding properties of various materials, including traditional and modern alloys, several gaps remain. Existing studies have largely focused on conventional shielding materials like lead and their well-established properties (Hamad, 2023). However, there is a need to explore and compare the performance of newer alloys, particularly Iron-based and Nickel-based alloys with Cobalt compositions, in terms of photon attenuation and shielding efficacy. The current literature provides limited insights into the comprehensive evaluation of both linear and mass attenuation coefficients (LAC, MAC), half and tenth value layers (HVL, TVL), mean free path (MFP), and other crucial parameters across a wide photon energy range (0.001 MeV to 10 MeV) for these alloys (Alghamdi et al., 2024; Sakar et al., 2020). Additionally, there is insufficient understanding of the effective atomic number ( $Z_{eff}$ ) and electronic density ( $N_{eff}$ ) variations in these alloys and their impact on photon shielding efficiency.

This study addresses the aforementioned research gaps by evaluating the radiation shielding properties of Iron-based and Nickel-based alloys with Cobalt, focusing on key parameters such as LAC, MAC, HVL, TVL, MFP,  $Z_{eff}$ , and  $N_{eff}$  using Phy-X/PSD software. By providing a detailed comparison of these alloys, the research aims to identify materials with superior photon attenuation capabilities and stable performance across different energy ranges. Nickel-based alloys are expected to exhibit better photon absorption and attenuation efficiency, particularly at lower energies, compared to Iron-based alloys (Zhang et al., 2020; Moradi et al., 2024). This study's findings will contribute to the development of more effective radiation shielding materials, which are crucial for applications in nuclear energy, medical imaging, and radiation protection, thereby addressing the need for improved safety and efficiency in these fields (Gaber et al., 2024; Heidarian et al., 2024).

## Methods and materials

A user-friendly online tool, Photon Shielding and Dosimetry (PSD) software, available at <https://phy-x.net/PSD>, has been developed to calculate various parameters essential for shielding and dosimetry [29]. This software computes parameters such as linear

and mass attenuation coefficients (LAC, MAC), half and tenth value layers (HVL, TVL), mean free path (MFP), effective atomic number and electron density (Zeff, Neff), effective conductivity (Ceff), as well as energy absorption and exposure buildup factors (EABF, EBF). It provides data on shielding parameters across a continuous energy range from 1 keV to 15 MeV. Access to this software is free, though registration on the Phy-X platform is required (Sakar et al., 2020). The LAC and MAC are critical parameters for assessing the dosimetric and radiation shielding performance of materials. They indicate how likely photons are to interact with a material per unit thickness. According to Beer-Lambert's law, the intensities of a photon beam before ( $I_0$ ) and after ( $I$ ) passing through the shielding material, with a physical thickness ( $x$ ), follow exponential absorption patterns as described by Equation (1) and (2) (Usta & Tozar, 2020).

$$I = I_0 e^{-\mu x} \tag{1}$$

$$\mu_m = \frac{\mu}{\rho} = \frac{1}{\rho} x \times \ln\left(\frac{I_0}{I}\right) \tag{2}$$

here  $\mu$ ,  $\rho$ , and  $\mu$  represent the linear attenuation coefficient (LAC,  $\text{cm}^{-1}$ ), density ( $\text{g}/\text{cm}^3$ ), and total mass attenuation coefficient (MAC,  $\text{cm}^2/\text{g}$ ), respectively. The MAC ( $\mu_m$ ) is determined using the mixture rule, as given by Equations (3) (Akkurt, 2011).

$$\mu_m = \omega_1 \left(\frac{\mu}{\rho}\right)_1 + \omega_2 \left(\frac{\mu}{\rho}\right)_2 + \dots = \sum \omega_i \left(\frac{\mu}{\rho}\right)_i \tag{3}$$

The elemental composition data of the ceramic slabs, obtained during characterization, was used as the shielding material for the simulation study. The source and the ceramic sample were positioned 20 cm apart to match the experimental setup. The simulation measured the fluence at a distance of 100 cm from the source using the tally track parameter. The fluence values were then used to calculate the LAC. This calculated value was compared with the experimental measurements to determine any discrepancies. Once the experimental setup was validated, the simulation was repeated to assess additional shielding properties, including the HVL, MAC, and MFP. HVL measures the appropriate thickness of the absorbing material needed to reduce the radiation to half from the initial radiation and is expressed in equation (4) (Takai et al., 2018):

$$HVL = \frac{0.693}{\lambda} \tag{4}$$

where  $\lambda$  represents the MFP, and Equation (5) is employed to calculate the MFP, a key parameter for evaluating shielding properties:

$$MFP(\lambda) = \frac{0.693}{HVL} \tag{5}$$

The total molecular cross-section (MCS) of the ceramic composite is calculated from the MAC value, as outlined in Equation (6) (Takai et al., 2018):

$$MCS = \mu_m \sum_i \frac{f_i A_i}{N_A} \tag{6}$$

where  $N_A$  represents Avogadro's number and ACS is then determined from the MCS using Equation (7):

$$ACS = MCS \sum n_i \tag{7}$$

Additionally, the ECS for each individual element is calculated using equation (8):

$$ECS = \frac{1}{N_A} \times \sum_i \frac{A_i f_i (\mu_m)_i}{Z_i} \tag{8}$$

where  $f_i$  represents the fractional abundance of the  $i$ -th element, and  $Z_i$  is the atomic number of the  $i$ -th element. The effective atomic number of the composite is denoted by  $Z_{eff}$  as described in equation (9) (Takai et al., 2018):

$$Z_{eff} = \frac{ACS}{ECS} \tag{9}$$

The table 1 presents the composition and density of two different alloy systems: Cobalt-Iron (Co-Fe) and Nickel-Cobalt (Ni-Co), each with varying weight fractions. The compositions range from 20% to 80% in terms of the primary component, with the secondary component making up the remaining percentage.

For Cobalt-Iron (Co-Fe) alloys, the composition is 20% Cobalt and 80% Iron, with a density of 8.0792 g/cm<sup>3</sup>, 40% Cobalt and 60% Iron, with a density of 8.2844 g/cm<sup>3</sup>, 60% Cobalt and 40% Iron, with a density of 8.4896 g/cm<sup>3</sup> and 80% Cobalt and 20% Iron, with a density of 8.6948 g/cm<sup>3</sup>. For Nickel-Cobalt (Ni-Co) alloys, the composition is 20% Nickel and 80% Cobalt, with a density of 8.9008 g/cm<sup>3</sup>, 40% Nickel and 60% Cobalt, with a density of 8.9032 g/cm<sup>3</sup>, 60% Nickel and 40% Cobalt, with a density of 8.9048 g/cm<sup>3</sup> and 80% Nickel and 20% Cobalt, with a density of 8.9064 g/cm<sup>3</sup>. As the proportion of Cobalt increases, the density of the Co-Fe alloys also increases. This suggests that Cobalt is denser than Iron, and thus higher Cobalt fractions contribute to an overall increase in density. The Ni-Co alloys show very slight increases in density as the Nickel content increases, although the variations in density are minimal. This implies that both Nickel and Cobalt have similar densities, with Nickel being marginally denser. The density changes reflect how elemental composition affects material properties. These differences may also impact mechanical, magnetic, and thermal properties of the alloys, which are important for various industrial applications such as magnetic materials or structural components in engineering.

**Table 1:** Samples detail for experiment using Phy-X/PSD

Weight by Fraction (%)		Sample Code	Density (gcm <sup>-3</sup> )	Weight by Fraction (%)		Sample Code	Density (gcm <sup>-3</sup> )
Cobalt	Iron			Nickel	Cobalt		
20	80	Co20Fe80	8.0792	20	80	Ni20Co80	8.9008
40	60	Co40Fe60	8.2844	40	60	Ni40Co60	8.9032
60	40	Co60Fe40	8.4896	60	40	Ni60Co40	8.9048
80	20	Co80Fe20	8.6948	80	20	Ni80Co20	8.9064

## Results and Discussion

In this study, the radiation absorption properties of various alloy materials, particularly Nickel-based and Iron-based alloys, were evaluated using the Phy-X software. The key parameters calculated include the MAC, which measures the material's ability to attenuate or absorb radiation as a function of energy, ranging from 0.01 MeV to 10 MeV. Several findings were observed from the analysis shown in figure 1 to figure 9, particularly regarding the behavior of Nickel-based and Iron-based alloys across different energy levels. Nickel-based alloys were found to exhibit higher MAC values at lower energy levels compared to Iron-based alloys. This indicates that Nickel-based alloys are more effective in absorbing radiation at lower photon energies. The reason for this could be attributed to the atomic structure and electron configuration of Nickel. At low energies, photoelectric absorption dominates, and elements with higher atomic numbers, such as Nickel, tend to have higher photoelectric cross-sections. This leads to a higher probability of photon interactions, thus resulting in greater attenuation in the low-energy region. As the photon energy increases, the MAC for all alloys, including both Nickel-based and Iron-based ones, decreases. This is consistent with the behavior of most materials, as higher energy photons tend to interact less frequently with matter, resulting in a lower attenuation coefficient. The dominant processes in higher energy regions are Compton scattering and pair production, both of which have lower cross-sections than photoelectric absorption, leading to reduced attenuation. The MAC of Nickel-based alloys was observed to fluctuate more across the energy spectrum compared to Iron-based alloys as shown in figure 1. These fluctuations can be linked to the complex electronic structure of Nickel, which has unfilled d-orbitals. These unfilled d-orbitals allow for more variability in photon absorption at specific energy levels, contributing to the observed fluctuations in MAC values.

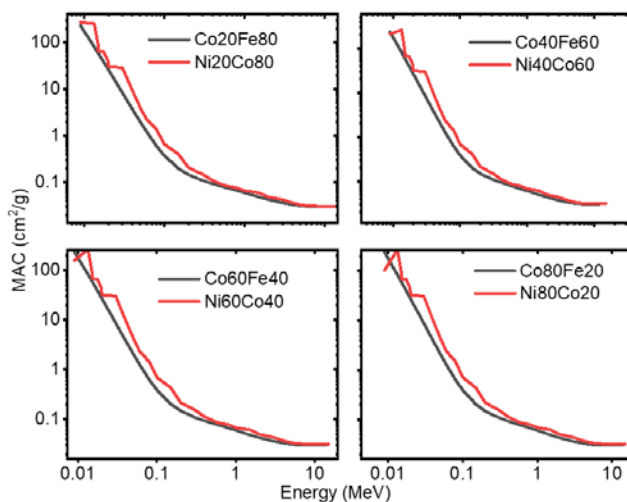


**Figure 1:** MAC of Ni, Co and Fe alloys

On the other hand, Iron-based alloys exhibited a smoother MAC curve, reflecting more consistent attenuation behavior across different energy levels. This suggests that Iron-based alloys have more stable electron configurations, leading to fewer abrupt changes in attenuation characteristics. For all alloys studied, the MAC decreased with increasing photon energy. This is because, at higher energies, the dominant interaction processes, such as Compton scattering, do not strongly depend on the atomic number. Therefore, as the photon energy increases, the material's ability to absorb radiation diminishes, resulting in lower attenuation. The nature of MAC with energy has similar nature obtained by Sayyed et al. (2020) with Ni-Based alloys using different software.

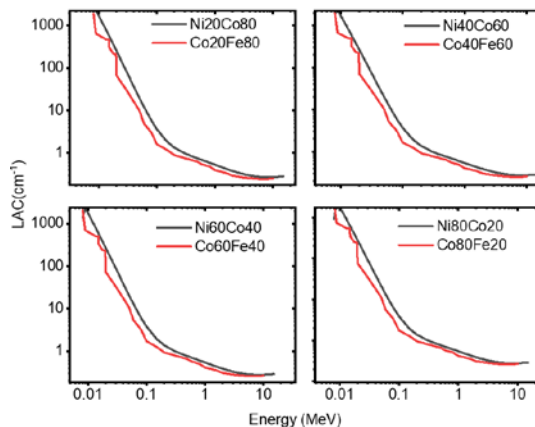


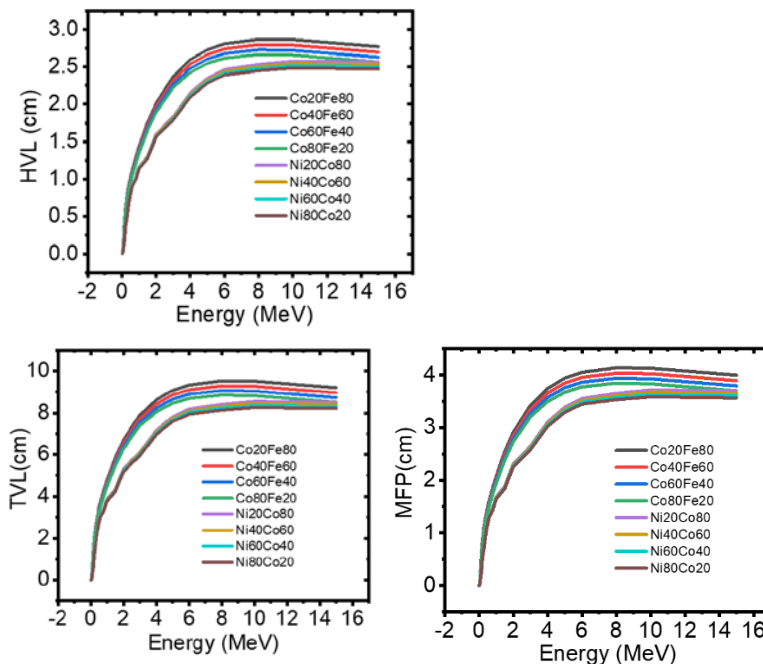
**Figure 2:** LAC of Ni, Co and Fe alloys

The LAC of Nickel-based alloys is higher at lower energy levels compared to Iron-based alloys, reflecting a similar trend observed for the MAC as shown in figure 2. The LAC, which depends on the material's density and its ability to attenuate photon radiation, follows the behavior of the MAC but accounts for the physical thickness of the material. The higher LAC values for Nickel-based alloys in the lower energy region imply that Nickel-based alloys are more effective at attenuating radiation at lower photon energies. This is because, in this energy range, photoelectric absorption dominates, and elements with higher atomic numbers (such as Nickel) tend to have larger cross-sections for photon absorption. Consequently, Nickel-based alloys, with a higher atomic number than Iron, exhibit greater attenuation capabilities in this region. Additionally, the density of the material plays a role, as Nickel has a higher density than Iron, contributing to the overall higher LAC.

Similar to MAC, the LAC shows significant deviation at lower energies compared to higher energy regions. At low photon energies, the interaction of photons with the material is more sensitive to changes in composition, leading to higher variability. This deviation diminishes as the photon energy increases, where the dominant interaction mechanism is Compton scattering, which is less dependent on atomic number and material composition, resulting in more consistent attenuation across all alloys. Interestingly, the Iron-based alloys

exhibit fluctuations in their LAC values, especially at lower energies. These fluctuations could be linked to the variations in electron density and the complexity of interactions between radiation and the atomic structure of Iron at low energy levels. The fluctuating nature might also indicate the influence of different interaction mechanisms at specific energy thresholds. In contrast, Nickel-based alloys demonstrate smoother LAC behavior, suggesting that the attenuation properties of Nickel alloys are more stable and less prone to fluctuations as energy varies. This stability could be due to the uniformity in the electronic structure of Nickel, which allows for more consistent photon interaction across different energy levels.

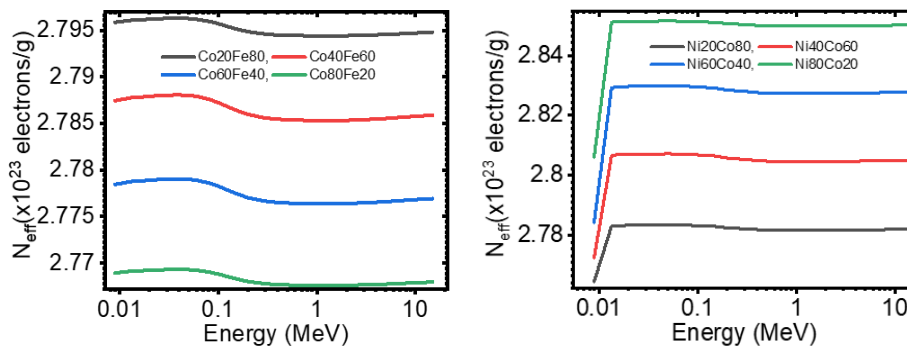
For both Nickel-based and Iron-based alloys, the LAC decreases as the photon energy increases. This trend reflects the shift from the photoelectric effect at lower energies to Compton scattering at higher energies, where photons interact less frequently with the material. As photon energy increases, the probability of interaction decreases, leading to reduced attenuation (and thus lower LAC values). The higher LAC of Nickel-based alloys in the low-energy region makes them more effective for radiation shielding or absorption at these energy levels. However, the fluctuations in LAC for Iron-based alloys suggest that these materials might be less reliable in providing consistent radiation attenuation, especially at low energies. Nickel-based alloys may thus be preferred in applications requiring stable and predictable attenuation properties across a range of energies. The decrease in LAC as photon energy increases is consistent with typical radiation-matter interactions and highlights the importance of material choice depending on the energy range of the radiation being encountered in applications such as nuclear power plant control rods.



**Figure 3:** HVL, TVL and MFP of Ni, Co and Fe alloys

For Iron-based alloys, it is observed that the HVL, TVL, and MFP decrease as the Iron concentration decreases and the Cobalt concentration increases. This indicates that adding more Cobalt to Iron-based alloys improves their radiation attenuation properties as shown in figure 3. Cobalt, with a higher atomic number than Iron, likely contributes to this enhancement by increasing the likelihood of photon interactions (particularly photoelectric absorption) at lower energies, resulting in a more efficient reduction of radiation intensity. For Nickel-based alloys, the HVL, TVL, and MFP increase with an increase in Nickel concentration. This suggests that as the proportion of Nickel increases, the alloy's effectiveness in attenuating radiation decreases slightly. This could be because the addition of more Nickel increases the alloy's density, but it also changes the interaction dynamics between photons and the material. Although Nickel is effective at absorbing radiation at low energies, the incremental increase in Nickel concentration does not necessarily enhance attenuation at higher energies more detail in figure 3. The nature of Nickel based alloys has similar nature of HVL, TVL and MEF (Aygün, 2021).

The behavior of HVL, TVL, and MFP as a function of photon energy and alloy composition indicates that Nickel-based alloys are generally more effective at attenuating radiation, particularly in the low-to-medium energy range (0-6 MeV), due to their lower values for HVL, TVL, and MFP. Iron-based alloys, on the other hand, are less effective, but their performance can be improved by adding Cobalt, which enhances the alloy's photon interaction properties. However, for Nickel-based alloys, increasing the Nickel concentration results in a slight decrease in attenuation effectiveness. These trends are critical in choosing the right material composition for radiation shielding or control rod applications, where efficiency across different energy ranges is crucial.



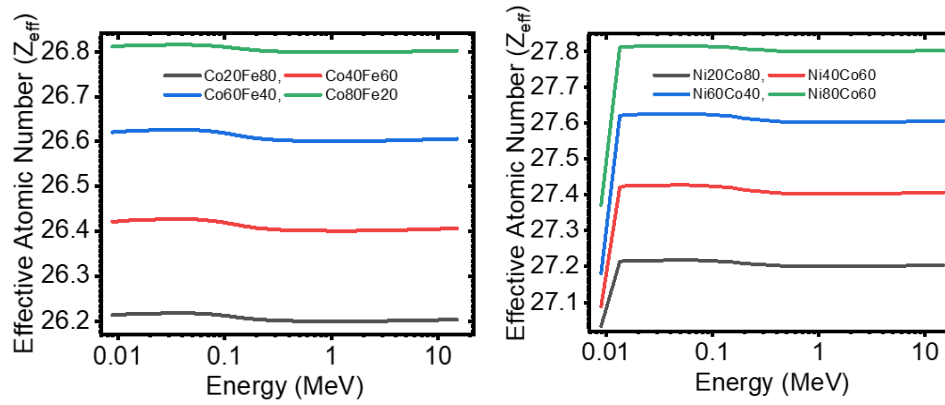
**Figure 4:** HVL, TVL and MFP of Ni, Co and Fe alloys

Figure 4 highlights the behavior of electron density for different alloys, specifically Iron-based and Nickel-based alloys, over a range of photon energies. The electron density, which refers to the number of electrons per unit mass of material, is crucial in determining the material's interaction with radiation, particularly in the photoelectric absorption process. The electron density in Iron-based alloys is observed to be higher in the lower energy region

(below 0.1 MeV), after which it starts to decrease as the photon energy increases. This behavior is indicative of the dominance of photoelectric absorption at low energies, where the probability of photon interaction is higher due to the dense electron population in these alloys. As energy increases, the electron density effect decreases, resulting in fewer interactions between the photons and electrons, leading to a decline in attenuation efficiency. This decline is gradual but noticeable around the 0.1 MeV. For Nickel-based alloys, the electron density sharply increases below 0.01 MeV, suggesting a high probability of photon interaction in this very low energy region. This sharp increase can be attributed to Nickel's higher atomic number compared to Iron, enhancing its ability to interact with low-energy photons. However, as the energy increases, the electron density decreases slightly, showing that the interaction between photons and electrons diminishes as the photon energy rises, especially in the Compton scattering and pair production regions.

For Iron-based alloys, the electron density increases with increasing Iron concentration. This is expected since Iron contributes to the electron population in the alloy, enhancing its overall capacity to attenuate radiation, particularly in the lower energy ranges where the photoelectric effect is significant. Conversely, the electron density decreases with increasing Cobalt composition in Iron-based alloys. The addition of Cobalt dilutes the electron concentration because Cobalt's atomic structure, while effective in higher energy ranges, does not contribute as much to electron density as Iron at lower energies. In Nickel-based alloys, the electron density increases with increasing Nickel composition. This trend aligns with the higher atomic number of Nickel compared to Cobalt, which enhances photon-electron interaction, particularly in the low-energy region. In contrast, as Cobalt composition increases in Nickel-based alloys, the electron density decreases, indicating that Nickel plays a more dominant role in enhancing electron interactions in these alloys, especially at low photon energies.

Iron-based oxides exhibit higher electron densities than Nickel-based oxides. This finding suggests that Iron-based alloys are better suited for low-energy photon attenuation, as their higher electron density ensures more interactions with incident photons. The order of electron density observed is in the range of  $10^{23}$  electrons per gram, which confirms the material's potential for effective radiation shielding, especially at lower photon energies. The behavior of electron density as illustrated in Figure 4 provides critical insights into the material's suitability for radiation attenuation. Iron-based alloys demonstrate a higher electron density in the low-energy region, making them more effective for radiation absorption at low photon energies. In contrast, Nickel-based alloys show a sharp increase in electron density below 0.01 MeV, making them ideal for very low-energy photon attenuation, though their effectiveness decreases at higher energies. The variations in electron density with changes in alloy composition further highlight the importance of material selection in optimizing radiation attenuation properties.



**Figure 5:** Effective atomic number of Ni, Co and Fe alloys

Figure 5 shows that the  $Z_{eff}$  of Nickel-based alloys is higher than that of Iron-based alloys, ranging from 27.1 to 27.8 for Nickel-based alloys and 26.2 to 26.8 for Iron-based alloys. This higher  $Z_{eff}$  in Nickel-based alloys suggests they are more efficient in photon interaction, especially at lower energy levels, where the photoelectric effect dominates. In contrast, Iron-based alloys, with their slightly lower effective atomic numbers, exhibit reduced photon absorption capabilities in the low-energy range but may perform better in higher energy regions. The variation in  $Z_{eff}$  is influenced by the proportion of elements in the alloy, with increasing Nickel content boosting photon interaction efficiency.

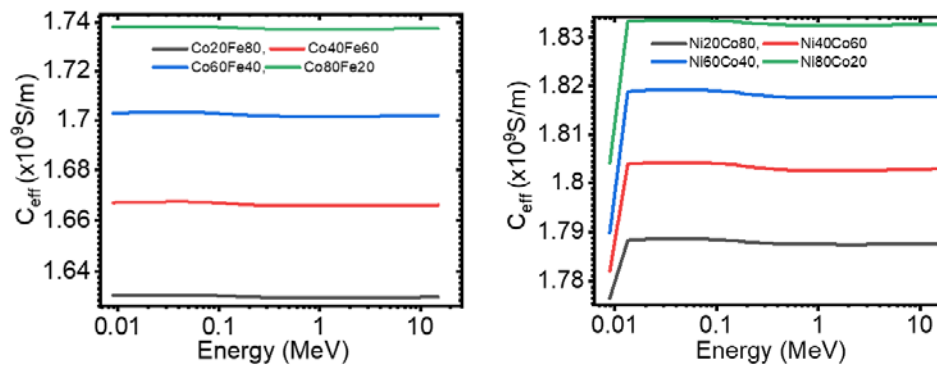


**Figure 6:** Effective conductivity of Ni, Co and Fe alloys

Figure 6 illustrates the behavior of  $C_{eff}$  for Iron-based and Nickel-based alloys as a function of incident photon energy. This parameter is essential for understanding how these materials respond to radiation, especially in applications where electrical conductivity is crucial alongside radiation shielding. The  $C_{eff}$  of Iron-based oxides remains almost constant across the increasing photon energy range, with values in the order of  $(1.50 \text{ to } 1.74) \times 10^9 \text{ S/m}$ . This consistency indicates that the electron mobility in Iron-based oxides is relatively unaffected by variations in incident photon energy, especially above 0.01 MeV. The stable conductivity is likely due to the inherent electrical properties of Iron and its oxides, which provide consistent electron flow regardless of the photon energy level. For Nickel-based

oxides, a significant fluctuation in  $C_{eff}$  is observed below 0.01 MeV. This fluctuation may be attributed to the increased photon interaction with the material at low energies, where the photoelectric effect dominates, causing variations in electron mobility. Once the photon energy exceeds 0.01 MeV, the  $C_{eff}$  stabilizes, similar to Iron-based oxides, indicating that the material's response becomes less dependent on energy fluctuations as higher-energy processes such as Compton scattering take precedence.

The  $C_{eff}$  of Iron-based oxides increases with the rising concentration of Cobalt. This trend can be explained by the fact that Cobalt improves the material's overall  $C_{eff}$ , likely due to enhanced electron mobility in the presence of Cobalt atoms. Cobalt's metallic nature contributes to greater free electron availability, thus enhancing conductivity. Conversely, in Nickel-based oxides, the  $C_{eff}$  decreases with increasing Cobalt concentration. This decline may result from a reduction in the number of free electrons available for conduction as Cobalt replaces Nickel in the alloy, leading to decreased overall electron mobility and hence lower conductivity.

The constant  $C_{eff}$  in Iron-based oxides with increasing photon energy suggests that these materials have stable electron mobility, possibly due to their crystalline structure, which does not fluctuate significantly with radiation exposure. The fluctuation in Nickel-based oxides at low energies may be due to their greater sensitivity to low-energy photon interactions, which temporarily alter the electron density and mobility. However, as energy increases and higher-energy photon interactions dominate, the material stabilizes. The effect of Cobalt on  $C_{eff}$  varies between Iron- and Nickel-based oxides due to differences in how Cobalt interacts with the base metals. In Iron-based oxides, Cobalt enhances  $C_{eff}$ , whereas in Nickel-based oxides, it reduces free electron availability, thereby lowering conductivity. Figure 6 highlights the stable  $C_{eff}$  nature of Iron-based oxides and the more variable  $C_{eff}$  of Nickel-based alloy at lower energies, influenced by the photon interaction mechanisms and the alloy composition.

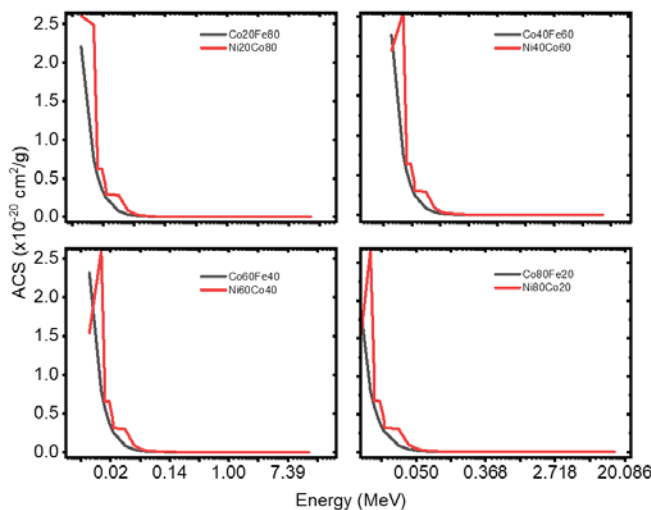
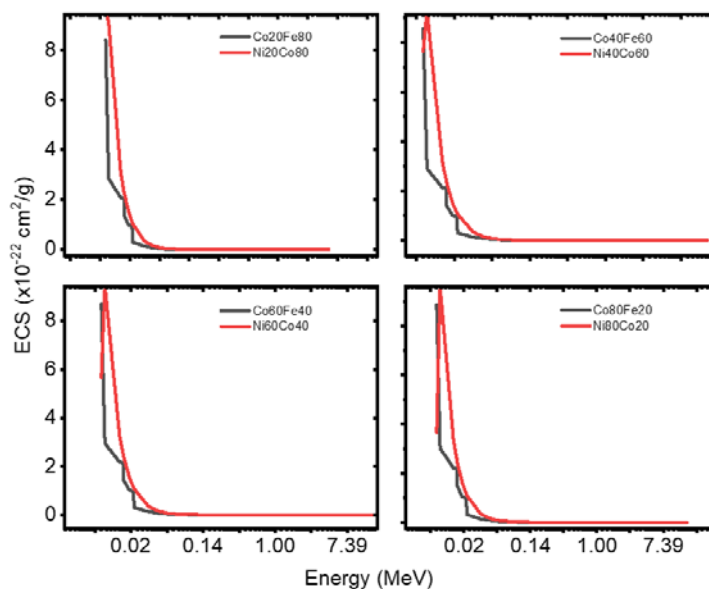


Figure 7: ACS of Ni, Co and fe alloys

Figure 7 demonstrates the behavior of the ACS for Iron-based and Nickel-based alloys in response to increasing photon energy. The ACS is a critical parameter that measures the probability of photon interaction with a material, and it directly influences how effectively a material can absorb or scatter radiation. The ACS decreases as the photon energy increases for both Iron- and Nickel-based alloys. This trend is typical because at higher energies, photons are more likely to pass through the material without interacting, resulting in a reduced probability of absorption or scattering. For Iron-based alloys, the decrease in ACS is smooth and consistent as photon energy increases. This steady decline suggests that the interaction of photons with Iron-based alloys becomes less probable at higher energy levels, but the reduction in interaction probability is gradual. This smoothness may reflect the relatively uniform distribution of atomic sites available for interaction within the Iron-based alloy structure.

In contrast, Nickel-based oxides show significant fluctuations in ACS, particularly in the lower energy region below 0.085 MeV. This fluctuation may be due to the stronger photoelectric effect in Nickel, which leads to variations in photon interaction rates. At lower energies, photons are more likely to be absorbed or scattered due to the higher interaction cross-section in Nickel-based materials, resulting in greater variability in ACS. Once the energy increases beyond this threshold, the interaction probability stabilizes, and ACS becomes almost constant. The ACS of Nickel-based alloys is generally higher than that of Iron-based alloys. This indicates that Nickel-based alloys have a higher probability of photon interaction, meaning that photons are more likely to be absorbed or scattered when they encounter Nickel-based materials. This could be due to the denser electron cloud in Nickel-based alloys, which increases the likelihood of interaction. A higher ACS also implies that the interaction region is larger for Nickel-based alloys, meaning that photons can interact with the material even when passing at a relatively larger distance from the atomic nuclei. The ACS indicates the region within which a photon is likely to interact with the alloy. A higher ACS, as observed for Nickel-based alloys, means that the photon interaction region is more extensive, allowing photons to interact even at a greater distance from the atomic centers. In contrast, a lower ACS (seen more in Iron-based alloys at higher energies) suggests that photon interaction is limited to a smaller region, and interaction only occurs when the photon is in close proximity to the atomic nuclei of the alloy. The findings from Figure 7 suggest that Nickel-based alloys are more effective at interacting with photons, particularly at lower energies, as indicated by their higher and more variable ACS. In contrast, Iron-based alloys exhibit a smoother decline in ACS, reflecting a more stable interaction pattern as photon energy increases. The ACS values for both types of alloys become nearly constant at higher photon energies, indicating that photon interaction probability reaches a plateau at these energies. This behavior reflects the material's capacity to absorb and scatter radiation and is vital for applications requiring precise control over photon interactions.



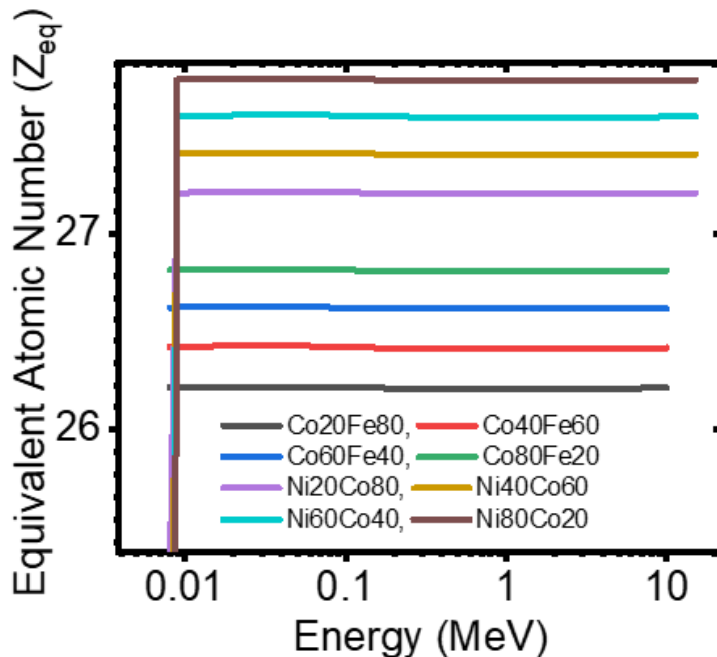
**Figure 8:** Electronic cross section of Ni, Co and Fe alloys

Figure 8 illustrates the variation of ECS for Nickel-based and Iron-based alloys as the photon incidence energy increases. ECS measures the likelihood of a photon interacting with an electron within the material, providing insight into the material's ability to absorb or scatter photons. The ECS for both Nickel- and Iron-based alloys decreases as the photon energy increases. This behavior is expected because higher-energy photons have greater penetration capabilities and are less likely to interact with electrons. At higher energies, photons are more likely to pass through the material without interacting, resulting in a decrease in ECS. For Nickel-based alloys, the ECS decreases smoothly across the photon energy range. This smooth decline indicates a consistent reduction in the likelihood of photon-electron interactions as energy increases. The steady behavior suggests that the electron density and distribution in Nickel-based alloys allow for a more uniform interaction pattern, particularly at low photon energies. In contrast, Iron-based alloys exhibit significant fluctuations in ECS, especially in the lower energy region below 0.14 MeV. These fluctuations may result from variations in electron density or structural irregularities in the Iron-based alloys that cause inconsistency in photon-electron interaction rates. This fluctuating nature implies that at lower energies, the interaction probability is more variable in Iron-based materials, potentially due to the complex arrangement of electrons in the alloy.

The ECS of Nickel-based alloys is generally higher than that of Iron-based alloys. This suggests that Nickel-based alloys provide a larger interaction region for photons, meaning they are more likely to absorb or scatter photons. A higher ECS indicates that photons can interact with electrons within the alloy over a larger distance, increasing the material's efficiency in photon-electron interactions. As with the ACS, a higher ECS in Nickel-based alloys means that the photon interaction region is larger, allowing photons to interact with electrons even when they are not in close proximity to the electron cloud. In

contrast, a lower ECS in Iron-based alloys means that photon-electron interactions are only likely to occur when photons are closer to the electron density within the material. This behavior influences the material’s ability to scatter or absorb photons efficiently.

At higher photon energies, beyond 0.14 MeV, the ECS for both Nickel- and Iron-based alloys becomes almost constant. This plateau indicates that at higher energies, the probability of photon-electron interactions stabilizes and is less influenced by further increases in energy. This suggests that, in this energy range, both Nickel- and Iron-based alloys have similar capacities to interact with photons, and the material differences become less pronounced. The ECS findings in Figure 8 show that Nickel-based oxides have a higher and more consistent photon-electron interaction probability compared to Iron-based alloys, especially at lower energies. The fluctuations in ECS observed for Iron-based alloys in the lower energy region suggest variable electron interaction patterns, while Nickel-based alloys exhibit a smoother behavior. At higher photon energies, the ECS for both alloys stabilizes, indicating a reduced impact of energy on the interaction probability, with Nickel-based alloys still maintaining a larger interaction region than Iron-based alloys. These insights are essential for applications where efficient photon-electron interaction is required.



**Figure 9:** Equivalent atomic number of Ni, Co and Fe alloys

Figure 9 illustrates the variation of the  $Z_{eff}$  for different alloys as a function of photon energy.  $Z_{eff}$  is an important parameter that reflects the average atomic number of a material, considering its ability to interact with photons.  $Z_{eff}$  remains relatively constant for all alloys when the photon energy exceeds 0.01 MeV. This stability indicates that at higher photon energies, the material's effective atomic number does not significantly change, suggesting that the overall interaction properties of the material are less influenced by

variations in photon energy. Below 0.01 MeV,  $Z_{\text{eff}}$  sharply increases, reaching a maximum before stabilizing with minimal fluctuations. This sharp increase reflects a higher probability of photon interactions at lower energies, where the material's effective atomic number becomes more pronounced. The increase in  $Z_{\text{eff}}$  at these lower energies is likely due to the enhanced interaction cross-section of photons with the electrons in the material. The  $Z_{\text{eff}}$  of Nickel-based alloys is generally higher than that of Iron-based alloys. A higher  $Z_{\text{eff}}$  indicates a greater effective atomic number, which suggests that Nickel-based materials have a higher electron density or more substantial interaction capability with photons. This higher  $Z_{\text{eff}}$  implies that Nickel-based alloys are more effective at absorbing or scattering photons due to their greater  $Z_{\text{eff}}$ .

For Nickel-based alloys,  $Z_{\text{eff}}$  increases as the cobalt concentration decreases. This is because, as cobalt is reduced, the proportion of Nickel, which has a higher atomic number, becomes more significant. Therefore, the overall effective atomic number of the alloy increases with a lower concentration of cobalt. Conversely, for Iron-based alloys,  $Z_{\text{eff}}$  decreases with a decrease in cobalt concentration. This occurs because reducing cobalt content in Iron-based alloys reduces the proportion of elements with higher atomic numbers, leading to a lower effective atomic number. After reaching a maximum value below 0.01 MeV, the  $Z_{\text{eff}}$  becomes almost constant with very little fluctuation. This indicates that once the lower energy threshold is surpassed, the  $Z_{\text{eff}}$  stabilizes, suggesting that the photon interaction characteristics of the alloys are consistent at energies above this threshold. Figure 9 reveals that Nickel-based alloys exhibit a higher effective atomic number compared to Iron-based alloys, especially at lower photon energies where  $Z_{\text{eff}}$  increases sharply before stabilizing. The concentration of cobalt in the alloys affects  $Z_{\text{eff}}$  differently for Nickel and Iron-based alloys: decreasing cobalt concentration increases  $Z_{\text{eff}}$  in Nickel-based alloys but decreases it in Iron-based alloys. Beyond 0.01 MeV,  $Z_{\text{eff}}$  remains relatively constant, indicating a stable interaction characteristic for both types of alloys at higher energies. This information is crucial for understanding the materials' performance in applications involving photon interactions, such as radiation shielding and detection.

## Conclusion

In conclusion, the study highlights significant variations in radiation interaction properties among Iron-based and Nickel-based alloys with Cobalt. Iron-based alloys exhibit increased electron density with higher Iron concentrations, enhancing low-energy photon attenuation, while Cobalt reduces this density due to its lower electron contribution. Conversely, Nickel-based alloys show improved electron density with increased Nickel content but reduced density with higher Cobalt levels, underscoring Nickel's dominance in electron interactions.  $Z_{\text{eff}}$  reveals that Nickel-based alloys are generally more efficient at low-energy photon interactions compared to Iron-based alloys. Effective conductivity remains stable in Iron-based alloys but fluctuates in Nickel-based alloys at low energies. Atomic and electronic cross-sections indicate that Nickel-based alloys offer higher interaction probabilities at lower energies, though both types stabilize at higher photon energies. These

insights are crucial for optimizing materials in radiation shielding and photon detection applications, with Nickel-based alloys showing superior performance at lower energies.

## References

- Sayyed, M.I.; Mohammed, F.Q.; Mahmoud, K.A.; Lacomme, E.; Kaky, K.M.; Khandaker, M.U.; Faruque, M.R.I. Evaluation of Radiation Shielding Features of Co and Ni-Based Superalloys Using MCNP-5 Code: Potential Use in Nuclear Safety. *Appl. Sci.* 2020, *10*, 7680. <https://doi.org/10.3390/app10217680>
- Aygiin, B. (2021). Neutron and gamma radiation shielding Ni based new type super alloys development and production by Monte Carlo Simulation technique. *Radiation Physics and Chemistry*, *188*, 109630.
- Takai, Z. I., Kaundal, R. S., Mustafa, M. K., Asman, S., Idris, A., Shehu, Y., ... & Said, M. (2018). Gamma ray and FTIR studies in zinc doped lead borate glasses for radiation shielding application. *Materials Research*, *22*, e20180404
- Akkurt, I. (2011). Determination of effective atomic number and electron density of chitin by gamma-ray attenuation. *Int J Phys Sci*, *6*, 5048-50.
- Usta, M., & Tozar, A. (2020). The effect of the ceramic amount on the radiation shielding properties of metal-matrix composite coatings. *Radiation Physics and Chemistry*, *177*, 109086.
- Heidarian, A., Naderi-Samani, H., Razavi, R. S., Jabbari, M. N., & Naderi-Samani, E. (2024). Synthesis of nickel particles for use in nickel/silicone rubber composites for the application of electromagnetic interference shielding gaskets. *Heliyon*, *10*(2).
- Pan, J., Wang, C., Wang, Z., Zhang, C., Fang, L., Li, J., ... & Xiao, X. (2024). Microstructure characteristics and properties of a novel Ni-based alloy for thermal neutron and gamma ray co-shielding. *Materials Characterization*, *210*, 113840.
- Gaber, E. A., Hussien, S. A., Saad, E. M., & Mahmoud, A. E. R. (2024). Effect of Bi<sup>3+</sup> on the structural, optical and simulate  $\gamma$ -radiation shielding features of borate glasses doped nickel ions. *Radiation Physics and Chemistry*, *218*, 111579.
- Ölçen, K. K., & Dikici, T. (2024). Evaluation of the shielding effectiveness of electrodeposited Zn–Ni, Zn–Co, Ni–Co, and Zn–Ni–Co alloy coatings. *Journal of Materials Science: Materials in Electronics*, *35*(19), 1376.
- Ramakrishna, B. N., Pasha, A., & Khasim, S. (2024). Improved broadband electromagnetic interference shielding and strain sensing properties of multifunctional reduced graphene oxide/iron–cobalt ferrite composites. *Journal of Materials Science: Materials in Electronics*, *35*(1), 48.
- Alghamdi, A. A., Maatouk, A., Almotawa, R. M., Sadeq, M. S., Abdel-Fattah, E., & Abdo, M. A. (2024). Enhancement of photocatalytic degradation stability and radiation shielding ability of Cr-substituted zinc-copper nanoferrites. *Radiation Physics and Chemistry*, *225*, 112111.
- Moradi, H., Nasouri, K., & Askari, G. (2024). Effect of morphology and microstructure of NiCo nanoparticles on the electromagnetic shielding behavior of flexible and durable NiCo-coated carbon fibers. *Journal of Materials Science: Materials in Electronics*, *35*(1), 89.
- Büyükyıldız, M., Thakur, S., Levet, A., & Kaur, P. (2024). Gamma-ray attenuation properties of some heavy metal ferroalloys for potential applications. *Progress in Nuclear Energy*, *176*, 105382.

- Aslam, R., Serdaroglu, G., Zehra, S., Verma, D. K., Aslam, J., Guo, L., ... & Quraishi, M. A. (2022). Corrosion inhibition of steel using different families of organic compounds: Past and present progress. *Journal of Molecular Liquids*, 348, 118373.
- Şakar, E., Özpolat, Ö. F., Alım, B., Sayyed, M. I., & Kurudirek, M. (2020). Phy-X/PSD: development of a user friendly online software for calculation of parameters relevant to radiation shielding and dosimetry. *Radiation Physics and Chemistry*, 166, 108496.
- Aygun, M., Aygun, Z., & Ercan, E. (2023). Radiation protection efficiency of newly produced W-based alloys: Experimental and computational study. *Radiation Physics and Chemistry*, 212, 111147.
- Zhang, Y., Cui, K., Fu, T., Wang, J., & Qie, J. (2020). Synthesis WSi<sub>2</sub> coating on W substrate by HDS method with various deposition times. *Applied Surface Science*, 511, 145551.
- Hamad, M. K. (2023). Evaluation of photon shielding properties for new refractory tantalum-rich sulfides Ta<sub>9</sub> (XS3) 2 alloys: a study with the MCNP-5. *Annals of Nuclear Energy*, 184, 109687.